16th World Conference on Earthquake Engineering, 16WCEE 2017
Santiago Chile, January 9th to 13th 2017
Paper N°4235
Registration Code: S-L1464683865

EXPERIMENTAL STUDY ON THE SEISMIC PERFORMANCE OF TYPICAL EXISTING REINFORCED CONCRETE BRIDGE PIERS WITH HOLLOW RECTANGULAR SECTIONS

P. Cassese[(1)], P. Ricci[(2)], G. M. Verderame[(3)], G. Manfredi[(4)]

[(1)] *Ph.D. Candidate, Department of Structures for Engineering and Architecture, University of Naples Federico II, paolino.cassese@unina.it*
[(2)] *Research Fellow, Department of Structures for Engineering and Architecture, University of Naples Federico II, paolo.ricci@unina.it*
[(3)] *Associate Professor, Department of Structures for Engineering and Architecture, University of Naples Federico II, verderam@unina.it*
[(4)] *Full Professor, Department of Structures for Engineering and Architecture, University of Naples Federico II, gaetano.manfredi@unina.it*

Abstract

In economically advanced countries, particularly in Europe and Italy, most of existing bridges have been constructed prior to 1980, before the advancement in earthquake engineering principles and the introduction of adequate seismic codes. These aspects, in combination with the strategic role of bridges in post-earthquake emergency management, specifically for the highway bridges, lead to the need to improve the assessment of the seismic capacity of existing bridge structures. Generally, important bridges have reinforced concrete hollow section piers, economically attractive. Recent main earthquakes around the world have highlighted the inadequate seismic performance of existing hollow piers, mainly due to poor structural detailing and small web thickness. Few experimental contributions are present in literature about bridge piers designed according to obsolete codes.

This study concerns an experimental campaign on poorly designed bridge piers with typical transverse section geometry (hollow rectangular) and different aspect ratios. The specimens have been designed in order to be representative of the Italian bridge structures realized in the above-mentioned period, in particular about materials (poor concrete and high strength steel) and reinforcement (low longitudinal and transversal reinforcement ratio). Piers have been designed and realized in 1:4 scale. Quasi-static cyclic tests under displacement control have been performed with a constant axial load. Different failure modes have been observed: flexure and flexure-shear in particular, basically depending on the specimens' slenderness.

Design criteria, adopted setup and experimental results are described and discussed.

Keywords: existing reinforced concrete bridges; experimental assessment, failure modes.

1. Introduction

In economically advanced countries, particularly in Europe and Italy, most of existing bridges have been constructed prior to 1980, before the advancement in earthquake engineering principles and seismic design codes. Damages to highway bridges due to intense earthquake events have serious implications for the economic life of the interested area, with or without life threatening consequences. Therefore, the assessment of existing bridge structures is a very important issue.

Generally, important bridges have reinforced concrete (RC) hollow section piers, economically attractive because of several reasons including the larger moment-of-inertia than solid sections with a similar area, reduced inertia masses, saving of materials and equipment during construction, reduced problems related to the hydration of massive concrete. Moreover, recent principal earthquakes around the world have highlighted the inadequate seismic performance of existing hollow piers, mainly due to poor structural detailing and small web thickness.

Seismic bridge design philosophy is to pursue energy dissipation by ductile flexural hinges at the piers base [1], unlike columns used in building frames that are typically designed following the weak beam-strong column philosophy for seismic resistance [2]. Brittle shear failure of bridge piers clearly has to be prevented to avoid disastrous collapse, but special attention has to be paid also to shear strength degradation with increasing flexural ductility demand. In fact, shear resisting mechanisms typical of hollow RC columns are very similar to that characterizing tube sections, depending mainly on webs aspect ratio. About degradation mechanisms, small thickness limits the confined concrete core, crucial to seismic energy dissipation [3]. Another important issue related to hollow RC piers is that their seismic response is characterized by high shear deformations, comparable to ones typical of RC walls, which may represent also a considerable portion of global top displacement [4].

A large number of experimental studies about existing RC piers has been performed for solid cross-section piers, in particular circular ([5]-[9]) and rectangular ([10]-[11]). On the other hand, only quite recently some experimental attention has been paid to cyclic response of hollow piers, in fact relatively few experimental studies are present in literature, some related to large-scale tests and others to reduced scale tests. Among the first ones, ductility of hollow square piers with adequate details [12] and cyclic response of real case hollow rectangular existing piers characterized by lap-splices located within plastic hinge region [13] were investigated. During last ten years, different experimental studies have been carried out on reduced-scale hollow piers. Some were performed on piers with hollow square cross-section, investigating about the influence of different parameters on the seismic response (among others, axial load ratio, transverse reinforcement ratio, aspect ratio) [14]. Others were carried out on hollow rectangular cross-sections piers, with only different stirrups arrangement [4].

The present experimental study aims at contributing to the investigation about cyclic lateral response of RC existing bridge piers with hollow rectangular cross-section. To this aim, four reduced-scale hollow rectangular RC piers different for aspect ratio (equal to height of the column over section depth ratio) were tested under cyclic increasing loading and constant axial force. Fixed a unique cross-section, to obtain these four cases, two different specimen height values and two loading directions were considered. The specimens were intended to be representative of typical design practices in force in Italy before 1980s, so they were characterized by low percentage of longitudinal and transverse reinforcement, inadequate details of horizontal reinforcement and lack of appropriate confinement reinforcement. It is possible to identify two different goals of this experimental study, namely: (i) the evaluation of the influence of aspect ratio on the seismic response of existing hollow section piers, in particular on the failure mode; (ii) the experimental analysis of deformability contributions to the top displacement.

Two distinct failure modes were expected and experimentally confirmed, depending on the specimen slenderness (flexure mode for taller piers and flexure-shear for shorter ones). In the next sections, first a description of specimens and experimental program details is provided. Later, the global experimental response and the final damage states are presented and discussed. Finally, the main deformability contributions characterizing RC columns (i.e. flexure, shear and fixed-end-rotation) are evaluated and discussed.

2. Experimental program and setup

2.1 Test specimens and materials

Four specimens representing cantilever bridge piers with hollow rectangular cross section are considered in this experimental study. The main goal of the design procedure is to obtain specimens representative in all aspects, such as materials, geometry and reinforcement details, of the existing bridge columns typical of the Italian transport infrastructures realized before 1980. This is achieved starting from the results of an investigation on a large sample of Italian RC bridges [15] and some indications available in literature [16].

Among others, the parameters taken into account are cross-section shape, gravitational axial load ratio, geometrical longitudinal and transverse reinforcement ratios, mean values of materials strength. In order to allow for testing within the capacity of the laboratory, a scaling factor equal to 1:4 is introduced. All specimens are characterized by the same cross section and reinforcement details. Exterior dimensions of the rectangular hollow section are 600x400mm and thickness (t_w) is 100mm. The geometrical longitudinal reinforcement percentage (ρ_l) is equal to 0.88%, given by two layers of Φ8 bars, 18 and 10 along the external and internal edges respectively. The transverse reinforcement ratio (ρ_w) is equal to 0.12%, with Φ3 stirrups spaced at a distance of 12cm and 90-degrees end hooks. About materials, a poor concrete has been reproduced, with a mean value of compressive strength of 20.4MPa, evaluated on twelve 15x15x15cm^3 cubic samples. Aggregates dimensions have been defined in order to be representative, on one side, and compatible with the tight concrete cover (1cm) due to the small scale of the specimens, on the other. Steel with yielding strength of 505MPa and ultimate strength at approximately 620MPa was used for longitudinal bars. Yielding strength of transverse reinforcement steel is equal to 655MPa, and ultimate strength is equal to 690MPa. Applied axial load level is 5% of the compressive axial capacity, within the range typical of service conditions of Italian bridge piers [15]. The structural variable considered in this experimental program was piers aspect ratio (L_v/H), in which L_v is the shear span (pier height from the base to the loading point) and H is the section depth (dimension of the cross-section in the loading direction). Two piers have a height of 900mm and two of 1500mm. Each one is tested along one of the principal directions, so that four different values of the aspect ratio are considered. All scaled piers reproduce non-seismic design, typical of the considered period, thus resulting in poorly detailed reinforcement (no tie between opposite longitudinal bars and 90° hooks, thus lack of confinement). For the tested specimens, cyclic response and collapse mode are very sensitive to flexure-shear interaction, due to low transverse reinforcement ratio as well as the shape of the cross-section. Main properties of specimens and materials are identified in Table 1 and in Table 2 respectively.

Table 1. Specimens properties

Specimen Id	**L_v** (mm)	**B** (mm)	**H** (mm)	**Aspect Ratio (L_v/H)**	**t_w** (mm)	**ρ_l**	**ρ_w**
P1	1500	400	600	2.50	100	0.88%	0.12%
P2		600	400	3.75			
P3	900	400	600	1.50			
P4		600	400	2.25			

Terms B and H in Table 1 are dimensions respectively parallel and orthogonal to applied displacement. In Table 2, cylindrical compressive strength medium value (f_{cm}), rebars and stirrups diameter (D), steel yield and ultimate tensile strength (f_{ym}, f_{tm}) and hardening ratio (f_{tm}/f_{ym}) are reported.

Table 2. Material properties

Concrete	**Steel**			
(f_{cm}) (MPa)	**D** (mm)	**(f_{ym})** (MPa)	**(f_{tm})** (MPa)	**(f_{tm}/f_{ym})** (-)
17.0	8	505	620	1.23
	3	655	690	1.05

A rigid cap was realized on the top of the piers in order to distribute axial and lateral loads on section flanges. Footings are designed to prevent any local damage. Plan and elevation views are illustrated in Fig. 1.

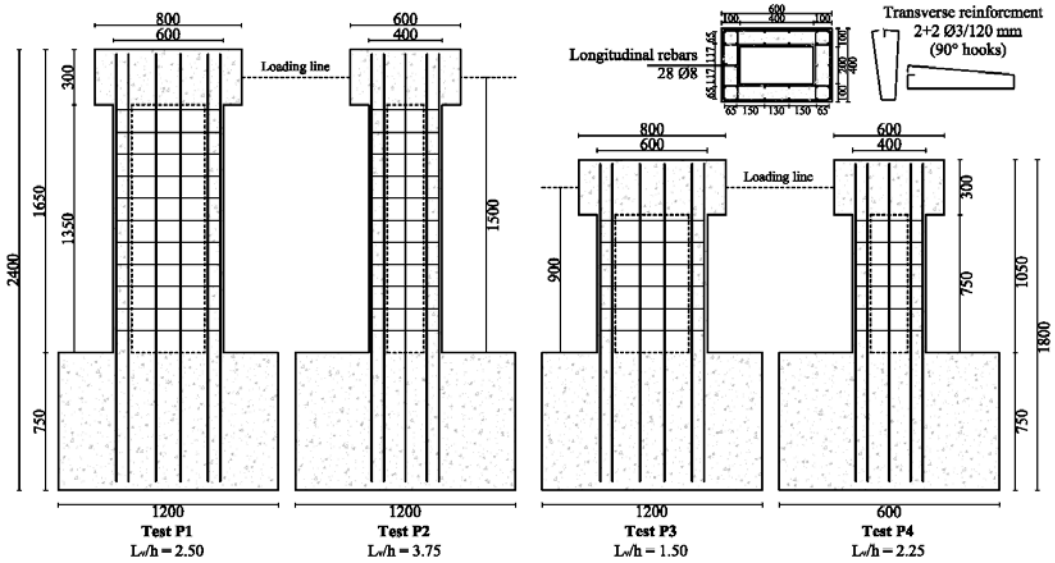

Fig. 1 – Geometry and reinforcement details

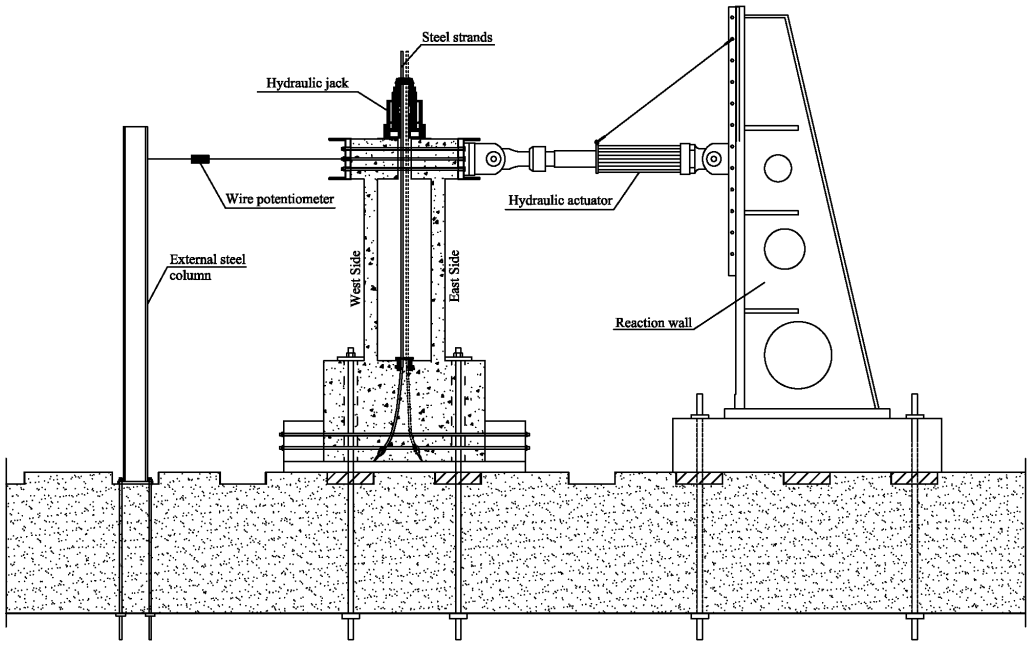

Fig. 2 – Test setup scheme

2.2 Test Setup

All tests were performed in quasi-static regime by applying horizontal displacement cycles along the centerline of the pile cap by a hydraulic actuator under displacement control. The actuator-to-specimen connection is schematized as a hinge constraint that does not restrain the rotation of the top during the test.

Axial load was applied to the test unit by means of a closed system consisting of 3 post-tensioned high strength Φ15.7 steel strands, fixed on the bottom side by means of anchorages embedded in the foundation concrete. A full height hole is realized in the cap in order to allow strands crossing the specimen. On the top, between the anchorage plate of the strands and the cap top surface, a hydraulic jack was interposed, acting in

load control. The foundation was restrained to the laboratory string floor by four post-tensioned tempered steel bars avoiding any rotation or movement during the test. A global graphic scheme of the test setup is shown in Fig. 2. In order to better understand the experimental results reported in the following sections, an orientation system is herein provided: specimens were tested along east–west directions (webs plain).

2.3 Test monitoring and loading scheme

Monitoring system was composed of two sub-systems, the former used for global measures, defining structural response of the specimen (forces and displacement), the latter for local measures, related to local deformation components associated with different response mechanism (see Section 4). Global system consisted of two load cells, respectively for horizontal and vertical forces, and a wire potentiometer fixed to an external steel column and connected to centroid of the pier cap (see Fig. 2). Since an important flexure-shear interaction was expected, and in order to investigate deeply about local deformation components coexisting in the specimens, an appropriate instrumentation was adopted along the pier height by using 8 + 8 Linear Potentiometers (LPs), installed on the two webs according the layout shown in Fig. 3a. In this way, two curvature cells and two shear deformation panels were realized. Flexural deformations and fixed-end-rotation at cantilever base was monitored by a couple of vertical Linear Variable Displacement Transducers (LVDTs), fixed to the center of the flanges end connected to the foundation upper surface (see Fig. 3b). In order to monitor longitudinal strain in steel reinforcement, strain gauges were mounted along corner longitudinal rebars and on the first two stirrups, along all four braces (see Fig. 3c). On the longitudinal rebars, the strain gauges were installed above the column base end and inside the footing, to control the development of plastic deformations. Finally, two cameras were installed on the two opposite side (i.e. north, south) at same distance in order to monitor cracking development.

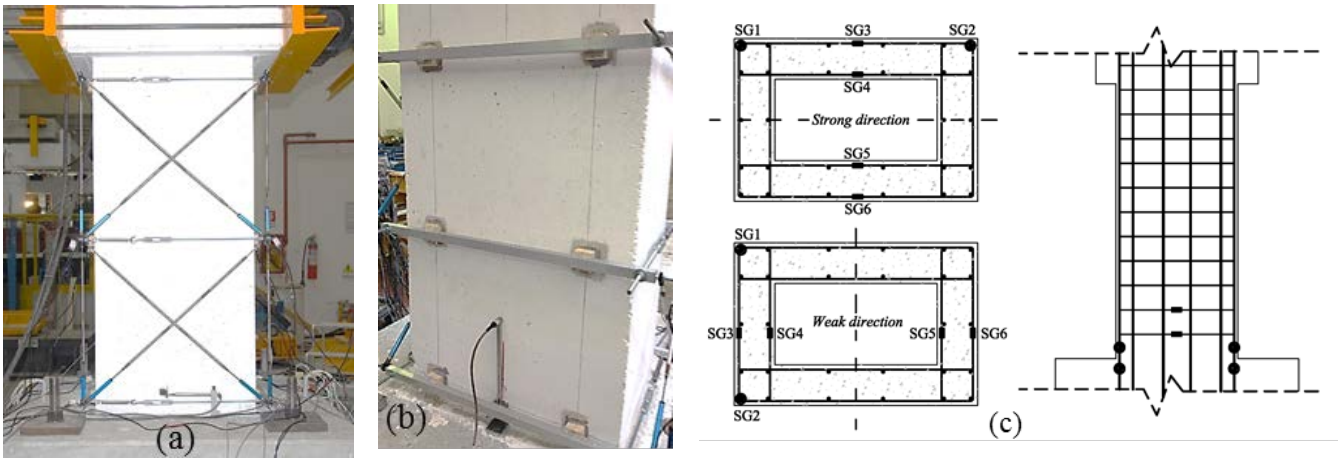

Fig. 3 – Instrumentation scheme: LPs (a), Base LVDTs (b) and Strain Gauges (SGs) (c)

Tests started applying slowly the vertical force until an axial load ratio equal to 0.05 was reached. Then, the specimens were subjected to quasi-static cycles of increasing displacement. The loading sequence consisted of three cycles at displacements of $1/3\Delta_y$, $2/3\Delta_y$, Δ_y, $2\Delta_y$, $4\Delta_y$, $6\ \Delta_y$, $8\ \Delta_y$, $10\ \Delta_y$, $12\ \Delta_y$, where Δ_y is the theoretical yielding displacement, unless failure occurred earlier. It is worth noting that such displacement protocol corresponded to that measured from the internal transducer of the hydraulic actuator. Since the reaction system is affected by small spurious deformations (due mainly to backlashes and deformations of contrast system), actual specimen displacements do not match exactly those values, especially for lower level of drift. Anyway, all experimental considerations are based on the exact values obtained from the external potentiometer positioned at the level of the horizontal actuator axis.

3. Global response

In this Section, the evolution of observed damage with increasing imposed displacement is briefly described and lateral load-displacement response of tested specimens is analysed. The results are discussed for each specimen separately. Response curves, in terms of lateral load versus drift (i.e. top displacement-to-height ratio), and final damage states are reported in Fig. 4.

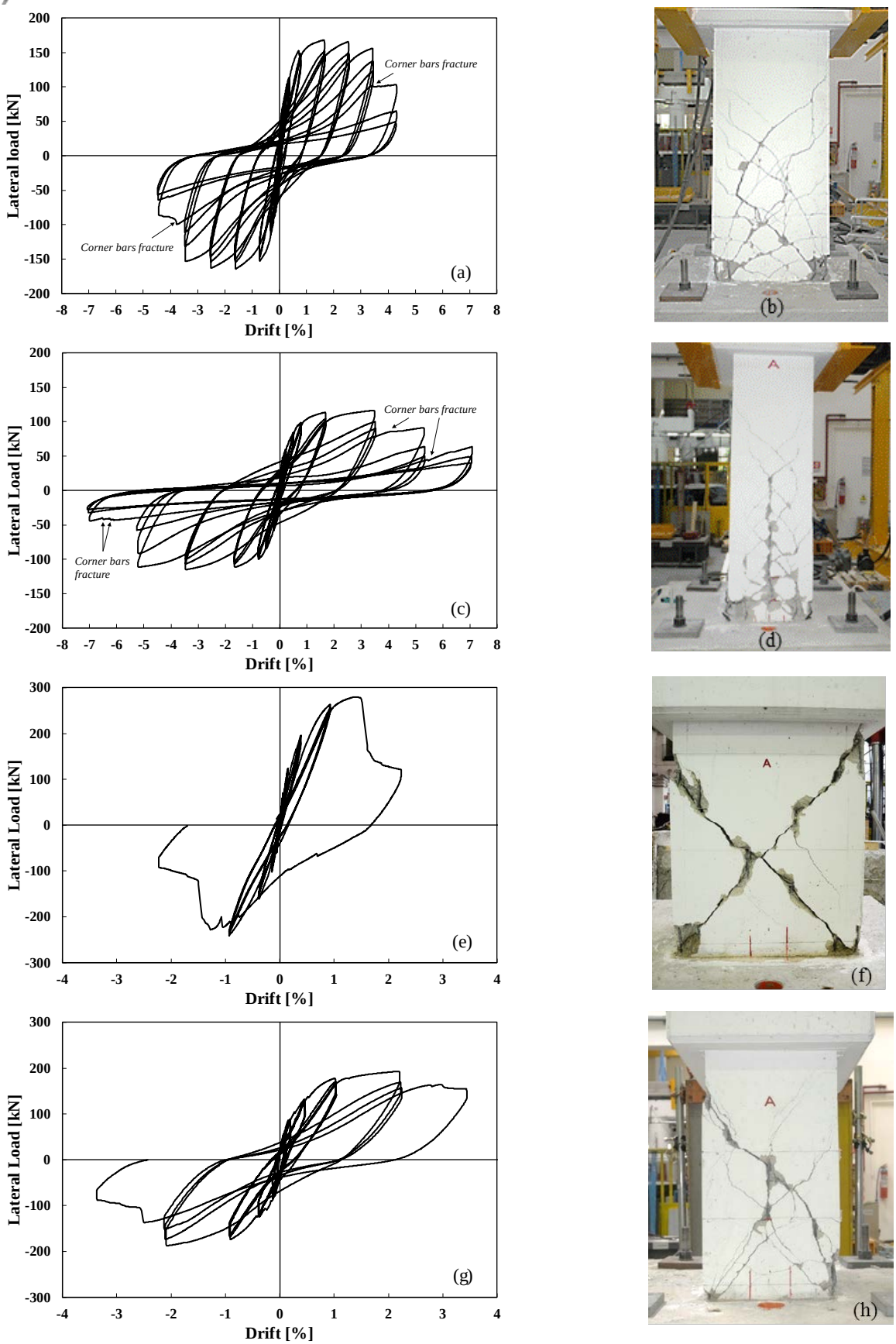

Fig. 4 – Lateral load versus drift cyclic response and final damage state, P1 (a,b), P2 (c,d), P3 (e,f), P2 (g,h)

3.1 Test P1

The results in terms of lateral load versus drift response and final damage state for Test P1 are reported in Fig 4a and Fig 4b respectively. Experimental response appears quite symmetric during the push-pull cycles. A first reduction of the initial stiffness was already observed during the first three cycles set, for a drift equal to 0.08%. Stiffness decreased gradually for a drift range between 0.21% and 0.34%, at which slight cracks appeared on the lower half of the element, initially as flexural horizontal cracks, later evolving along diagonal directions. A considerable stiffness reduction was observed during the fourth set of cycles, for a drift value of 0.76% and a force equal to about 153 kN. Specimen reached yielding condition, as confirmed by longitudinal bars strain measures provided by strain gauges located at the base of the test unit. Existing cracks increased their width, new flexural cracks formed up to a height of about 1000mm from the column base. Further shear cracks formed as extensions of flexural cracks on the upper part of the specimen. Peak load was reached for a drift equal to +1.68% for positive loading direction (push) and -1.63% for negative loading direction (pull). The corresponding peak values of top lateral load were +164 kN and -168 kN, respectively. During the cycles corresponding to peak load, the existing cracks extended and considerably increased their width. Damage at the base of the column developed quickly: vertical cracks appeared in concrete cover corners due to longitudinal bars buckling. The post-peak response was governed by flexure. In fact, it was characterized by a gradual degradation with a softening stiffness (calculated on the envelope of first cycles) equal to -7.3% and -6.7% of the initial stiffness, in positive and negative loading direction respectively. Experimental response was symmetric also in inelastic cycles. The inter-cycle strength drop developed from 10% to 24% from fourth to seventh loading step. During sixth cycles set, for a drift of 2.55%, flexural cracks at column base considerably widened and concrete cover corners completely spalled off. The subsequent cycles set (drift = 3.47%) was characterized by a significant concrete spalling together with significant buckling of longitudinal rebars within the distance between the base and the first layer of transverse reinforcement. During the last cycles set (drift = 4.40%), concrete of the compressed flanges was completely crashed and spalled. Longitudinal corner rebars failed in tension due to oligo-cyclic fatigue caused by buckling/tension cycles. In particular, this phenomenon occurred when the imposed drift overcame the maximum drift attained during the previous cycles set (see Fig 4a), and the associated increase in tension demand on longitudinal buckled bars led to their fracture, thus leading to a sudden intra-cycle strength drop/stiffness decrease in negative/positive direction.

3.2 Test P2

The results in terms of lateral load versus drift response and final damage state for Test P2 are reported in Fig 4c and Fig 4d respectively. Experimental response appears quite symmetric during the push-pull cycles only up to peak load, while post-peak phase is characterized by different evolutions in positive and negative load direction. Also in test unit P2, a first reduction of the initial stiffness was observed during the first three cycles set (drift = 0.23%). Hairline cracks were observed along the East and West specimen surfaces, at the first stirrups levels. Stiffness decreased gradually for a drift range between 0.50% and 0.79%, at which slight cracks appeared on the upper half of the element and the existing flexural cracks evolved along diagonal directions. Longitudinal rebars reached yielding strain value during the third loading step, as confirmed by the strain gauges located at the base of the test unit. A substantial stiffness reduction was observed during the fourth set of cycles (drift = 1.69%). Specimen reached yielding condition and damage state developed quickly: existing cracks increased their width, new flexural cracks formed and further shear cracks appeared as extensions of flexural in the central zone. Peak load was reached for a drift equal to 3.50% for both positive and negative loading direction, with a corresponding strength peak of 116 kN. During the cycles corresponding to peak load, existing cracks increased their width suddenly, diagonal ones in particular, which intersected themselves in correspondence of the central longitudinal bar, causing a concrete cover spalling along a vertical center line. Damage at the base of the column developed quickly: vertical cracks appeared on cover corners due to longitudinal bars buckling and concrete spalled off. Hysteretic curves were characterized by a considerable pinching effect. The post-peak response was asymmetric and governed by flexure. In fact, during sixth cycles set (drift = 5.25%) different load values were reached in positive and negative direction, equal to +91 kN and -111 kN respectively. Such an asymmetry was due to first longitudinal corner rebar failure in tension (because of oligo-cyclic fatigue). This phenomenon implicated a drop in strength (45% in push direction and 60% in pull). Softening stiffness values (calculated on the envelope of first cycles) were equal to -6% and -3% of the initial stiffness, in positive and negative loading

direction respectively. During the last cycles set, for a drift of 7.08%, compressed concrete between the base and the first stirrups layer completely crushed and spalled. Remaining longitudinal corner rebars failed in tension. Corresponding hysteresis loops were very narrow.

3.3 Test P3

The results in terms of lateral load versus drift response and final damage state for Test P3 are reported in Fig 4e and Fig 4f respectively. Experimental response appears slightly non-symmetric during the push-pull cycles. This effect, more evident with increasing drift, is associated with the shear cracking extension and reversal process. Once a set of cracks is open for a given loading direction, the reversal into the opposite direction is partially characterized by closing of the previously opened shear cracks. Therefore, for a given imposed horizontal displacement, a stiffness decrease is observed. Also in test P3, a first reduction of the initial stiffness was observed during the first three cycles set (drift = 0.06%). No cracks were observed along the specimen surfaces, but only at the base section. Stiffness decreased gradually for a drifts range between 0.17% and 0.41%, at which slight cracks appeared on the East and West specimen surfaces along first four stirrups layers and evolved quickly along diagonal directions toward compressed zone. In particular, two diagonal cracks formed from top to down opposite corners with an inclination angle of about 45 degrees. A substantial stiffness reduction was observed during the fourth set of cycles (drift = 0.93%). Longitudinal rebars reached yielding strain value, as confirmed by the strain gages located at the base of the test unit. Specimen reached yielding condition and damage state developed quickly: existing shear cracks increased their width and length, no flexural cracks formed and new slight shear cracks appeared as extensions of flexural ones in the central zone. It is noteworthy highlighting that, unlike test P1 and test P2, no considerable damage was observed on the base zone. Fifth cycles set (drift = 2.23%) was characterized by a single push/pull cycle. During pushing phase, for a drift value of +1.48%, drop in strength equal to 58% was observed, from +278 kN to +118 kN, at a drift value of +2.23%. Main shear crack opened suddenly up to a width of about 10 mm, along an ideal concrete strut with a medium inclination of about 42 degrees. A sliding between the upper and the lower part of the specimen was observed, with buckling of longitudinal rebars crossing the main diagonal crack. Shear sliding also caused buckling of the longitudinal rebars next to the base section with resulting concrete cover spalling. Pull phase was characterized by a lower stiffness. For a drift equal to -1.27% another drop in strength was observed (from -228 kN to -92 kN). Shear crack with a medium inclination of about 47 degrees opened suddenly, causing buckling in longitudinal rebars and concrete cover spalling.

3.3 Test P4

The results in terms of lateral load versus drift response and final damage state for Test P1 are reported in Fig 4g and Fig 4h respectively. Experimental response appears quite symmetric during the push-pull cycles. Also in test unit P4, a first reduction of the initial stiffness was observed during the first three cycles set (drift = 0.06%). No cracks were observed along the specimen surfaces, but only at the base section. Stiffness decreased gradually during second and third cycles sets, for a drift range between 0.17% and 0.43%. In fact, the second set was characterized by slight cracks on the East and West specimen surfaces along second and third stirrups layers, evolving quickly along diagonal directions toward compressed zone. Existing cracks increased their width during the third set, some flexural hairline cracks appeared next to the base and two wider diagonal cracks formed from top to down opposite corners with an inclination angle of about 38 degrees. A substantial stiffness reduction was observed during the fourth set of cycles (drift = 0.99%). Longitudinal rebars reached yielding strain value, as confirmed by the strain gages located at the base of the test unit. Specimen reached yielding condition and damage state developed quickly: existing shear cracks increase their width and length and new slight shear cracks appeared in the central zone, next to principal ones. Peak load values were reached, +193 kN and -188 kN, in positive and negative loading direction respectively. The inter-cycle strength drop developed from 5% to 19% passing from fourth to fifth loading step. Damage state evolved quickly: new shear cracks formed in the upper part, existing main diagonal cracks increased their width and extended reaching the base corners, causing concrete cover cracking. A clear fixed-end rotation was observed. Sixth loading step (drift = 3.40%) was characterized by one push/pull cycle. During pushing phase, for a drift value of +2.80%, response curve evolved along a horizontal slope, maintaining an about constant force value equal to +155 kN (equal to 80% of peak load) up to a drift of +3.40%. East-West principal diagonal crack opened suddenly. During the

following pull phase, for a drift value of -2.49%, a sudden strength drop was observed (from -137 kN to -87 kN). The loss in strength respect to global peak load was equal to 54%. Corresponding to this drop, West-East main shear crack, along an ideal concrete strut with a medium inclination of about 38 degrees, opened suddenly up to a width of about 10 mm. A sliding between the upper and the lower part of the specimen was observed, with buckling of longitudinal rebars crossing the shear crack. Shear sliding caused buckling of the longitudinal rebars next base section with resulting concrete cover spalling.

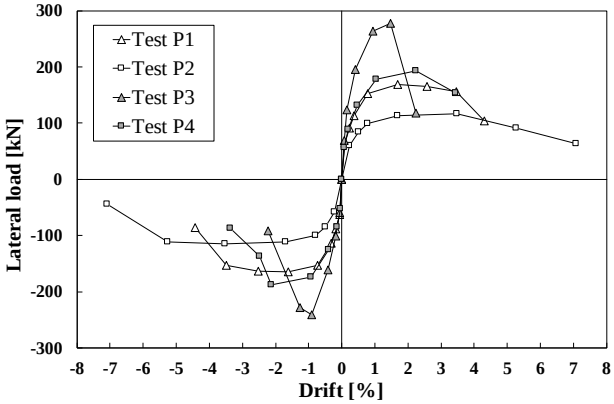

Fig. 5. Envelopes of lateral load versus drift response

Lateral load-drift envelopes corresponding to the first sub-cycles for each loading step are reported in Fig. 5 for all tests. Table 3 summarizes peak values of lateral force for both positive (V^+_{max}) and negative (V^-_{max}) loading directions with corresponding drifts (D^+_{max}, D^-_{max}), observed failure modes (F: flexure mode; FS: shear failure after flexural yielding) and "ultimate" drifts (D^+_u, D^-_u). Ultimate drifts values were evaluated as those corresponding to a strength reduction equal to 20% with respect to the peak load on the experimental backbone.

Table3. Peak and Ultimate Values

Specimen Id	**Aspect Ratio (L_v/H)**	**V^+_{max}** (kN)	**D^+_{max}** (%)	**V^-_{max}** (kN)	**D^-_{max}** (%)	**D^+_u** (%)	**D^-_u** (%)	**Failure Mode**
P1	2.50	168.3	1.68	-164.4	-1.63	3.80	-3.79	F
P2	3.75	116.6	3.48	-115.2	-3.53	5.15	-5.25	F
P3	1.50	277.7	1.48	-240.6	-0.92	1.74	-1.59	FS
P4	2.25	193.0	2.24	-187.5	-2.13	3.40	-2.97	FS

4. Local response: analysis of deformability contributions

Seismic response of RC elements with hollow sections, typical of bridge piers, can be governed by a considerable flexure-shear interaction, depending on their slenderness. Such an interaction leads to typical cracks layout on web surfaces, similar to slender cantilever walls. This deformation mechanism may represent a considerable portion of the global deflections, limiting ductile energy dissipation. In order to investigate this issue, an appropriate monitoring system was installed (see Fig.3).

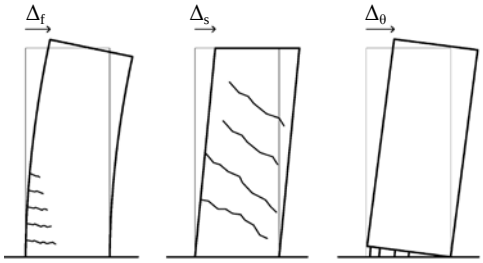

Fig. 6. Deformability contributions to total displacement

The top displacement of the specimens (Δ) can be interpreted as the results of three response mechanisms: flexure (Δ_f), shear deformation along webs (Δ_s) and fixed-end-rotation due to longitudinal bar slip at column base (Δ_θ) (see Fig. 6 and Eq. (1)). Assuming a uniform curvature distribution, Δ_f along the two curvature cells was calculated as the sum of the rotations measured by vertical LPs multiplied by corresponding distances from the top of the column (Eq. (2)). Strictly speaking, the fixed-end-rotation contribution Δ_θ is due to the slip from the foundation and it cannot be directly evaluated; instead, the *base rotation* θ_b is measured by the two LVDTs monitoring vertical deformation along the height h_b=50 mm from the base section. θ_b is associated to the base crack width including slip from element and from foundation, and to flexural deformation along h_b. The corresponding displacement Δ_b was calculated according to Eq. (3), similar to Eq. (2). Δ_s was estimated using Eq. (4), based on the hypothesis of small angles and uniform shear deformation over the measuring panel height. In Eqs. (2) – (4), h_i, h_j, l, d, are respectively heights, width and diagonal of the measuring panels; h_b is the height of first curvature cell, next to base section; $\delta_{o,i}$ and $\delta_{e,i}$, δ_1 and δ_2 are average values between north and south specimen surfaces of vertical and diagonal experimental measurements.

$$\Delta = \Delta_f + \Delta_b + \Delta_s \tag{1}$$

$$\Delta_f = \sum_{i=1}^{2} \theta_i \left[L_v - \left(\sum_{j=1}^{i-1} h_j + h_i / 2 \right) - h_b \right], \ \theta_i = \frac{\delta_{o,i} - \delta_{e,i}}{l} \tag{2}$$

$$\Delta_b = \theta_b \left(L_v - h_b / 2 \right) \tag{3}$$

$$\Delta_s = \frac{d}{2l} \left(\delta_1 - \delta_2 \right) \tag{4}$$

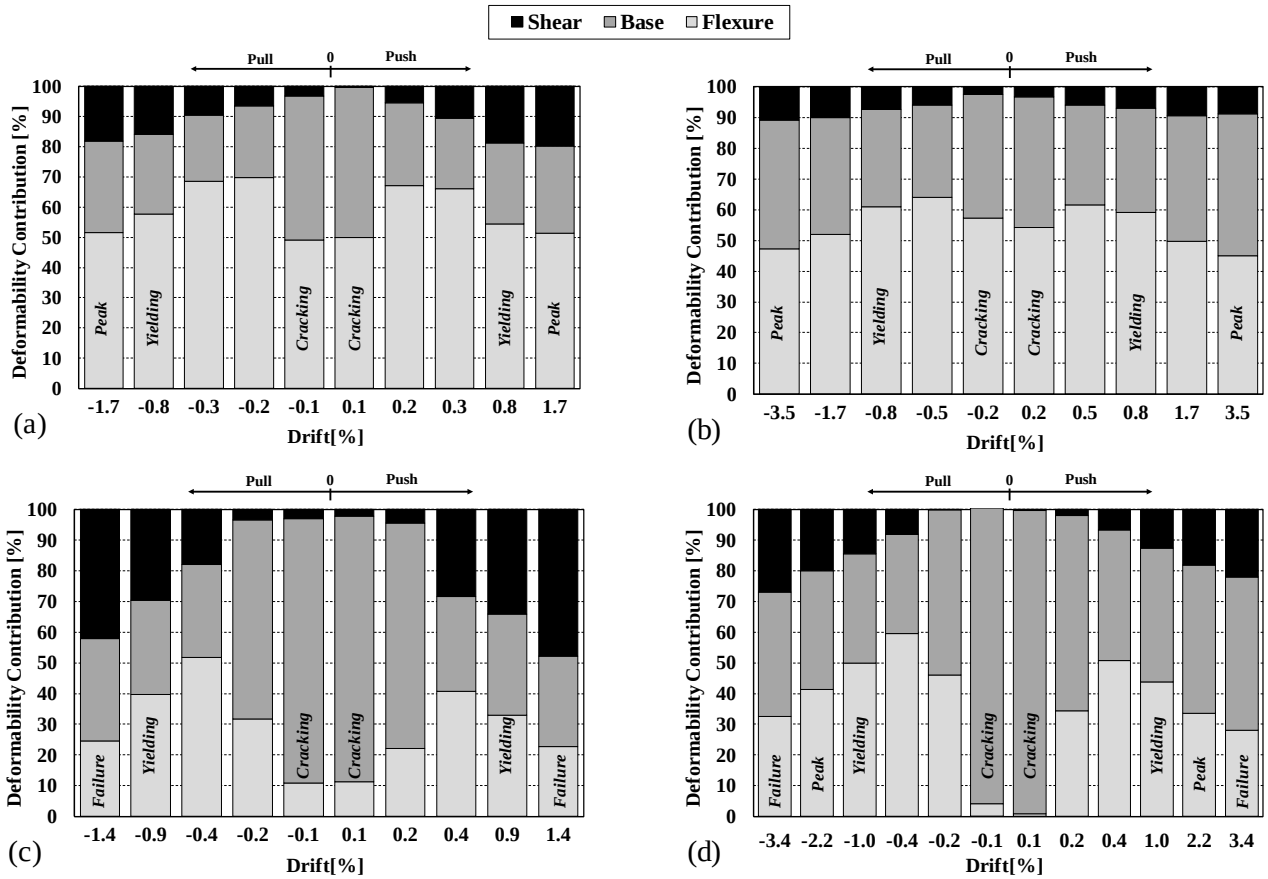

Fig. 8. Experimental deformability contributions to total displacement - P1(a), P2(b), P3(c), P4(d)

Fig. 8 shows deformability components as a function of the top displacement (until all measures can be considered as reliable and for first cycle at each drift level, both in positive and negative directions). Global symmetry of the response in push/pull direction is confirmed also in terms of local deformations.

For all tests, flexural deformability contribution (sum of Δ_b and Δ_f) was predominant respect to shear one. It is very interesting to note that for tall specimen (i.e. P1 and P2), flexural deformation was distributed over the height since from first cycle, with a cracking layout typical of slender element (balanced dark and light gray in figure). For short columns (i.e. P3 and P4), flexural deformation was initially concentrated at the base, with hairline cracks formed only at column/foundation interface (dark gray predominance in figure).

It seems possible to identify a relation between shear contribution to top displacement (Δ_s/Δ) and aspect ratio (L_v/H). In fact, for slenderest specimen (i.e. P2) maximum value of shear contribution is equal to 10.8%. For test units P1 and P4, characterized by similar aspect ratios (equal to 2.50 and 2.25 respectively), for a drift value corresponding to peak load, shear contribution is equal to 20.0% of the top displacement. The test P3 is characterized by higher shear deformations since first cycles. In fact, Δ_s/Δ ratio reached an average value of 31.9% at yielding cycle and 44.9% at shear failure.

5. Conclusions

In this work, experimental results of cyclic tests on reduced-scale RC bridge piers with rectangular hollow cross-section are shown and analyzed. Test units are representative of typical Italian bridge piers constructed prior 1980s, and they were designed without earthquake provisions (low transverse reinforcement ratio and inadequate seismic details). Given the cross-section and the reinforcement details, different aspect ratios were considered by changing height of the specimens and loading direction. Depending on the aspect ratio, different failure modes were expected, namely flexure failure for tall piers and shear failure after flexural yielding for short piers.

Experimental results, in terms of lateral load versus drift, and damage evolutions showed that:

- Tests P1 and P2, characterized by a higher aspect ratio ($L_v/H \geq 2.5$), showed flexural failure modes, with a cyclic response governed by ductile mechanisms. Damage states evolutions were typical of ductile members, with most of damage in non-linear phase located at base (concrete crushing, longitudinal rebars buckling).
- Test P3, characterized by an aspect ratio $L_v/H=1.5$, showed shear failure after flexural yielding. The cyclic response was typical of squat columns, governed by shear mechanisms. In fact, damage evolution was characterized by significant diagonal cracks since linear phase. Shear failure mode was characterized by a large drop in strength (of about 60% respect to maximum reached value) related to evident diagonal cracks opening, inclined of about 45 degrees.
- Test P4, characterized by an aspect ratio $L_v/H=2.25$, showed shear failure after flexural yielding. The cyclic response was characterized by flexure-shear interaction. In fact, during non-linear phase damage evolution was characterized initially by flexural cracks at the base, for drift values higher than test P3, and later by significant diagonal cracks, up to shear failure.

An experimental analysis of deformability contributions to the top displacement was performed, in order to better understand the relevance of taking into account shear deformations for bridge piers assessment. From experimental results, it seems possible to identify a relation between shear contribution to top displacement (Δ_s/Δ) and aspect ratio (L_v/H). In particular:

- For slenderest specimen P2, maximum value of shear contribution is equal to 10.8%, quite negligible.
- For test units P1 and P4, characterized by lower similar aspect ratios, about 20.0% of top displacement corresponding to peak load is due to shear deformations.
- For squat test units P3, shear deformability contribution to top displacement is about 32% and 45% respectively at yielding and peak load conditions.

The tests presented herein can provide a useful contribution to enlarge the relatively limited experimental database on existing hollow rectangular RC piers. In particular, the experimental analysis of all the sources of

deformability characterizing cyclic response can be a good reference for future studies related to the proposal/validation of nonlinear models for seismic assessment.

6. Acknowledgements

This work was developed under the financial support of STRESS S.c.a.r.l, STRIT Project "PON Ricerca e Competitività 2007-2013". This support is gratefully acknowledged.

7. References

[1] Priestley MN, Seible F, Calvi GM (1996). *Seismic design and retrofit of bridges*. John Wiley & Sons.

[2] Paulay T, Priestley MJN (1992): *Seismic Design of Reinforced Concrete and Masonry Buildings*. John Wiley & Sons.

[3] Kim IH, Sun CH, Shin M (2012). Concrete contribution to initial shear strength of RC hollow bridge columns. *Structural Engineering and Mechanics*, **41**°(1), 43-65.

[4] Delgado R, Delgado P, Pouca NV, Arêde A, Rocha P, Costa A (2009). Shear effects on hollow section piers under seismic actions: experimental and numerical analysis. *Bulletin of Earthquake Engineering*, **7**°(2), 377-389.

[5] Priestley MJN, Park R (1987). Strength and ductility of concrete bridge columns under seismic loading. *ACI Structural Journal*, **84°**(1), 61–76.

[6] Chai YH, Priestley MN, Seible F (1991). Seismic retrofit of circular bridge columns for enhanced flexural performance. *ACI Structural Journal*, **88**°(5), 572-584.

[7] Priestley MN, Seible F, Xiao Y (1994). Steel jacket retrofitting of reinforced concrete bridge columns for enhanced shear strength--Part 2: Test results and comparison with theory. *ACI Structural Journal*, **91**°(5), 537-551.

[8] Xiao Y., Ma R (1997). Seismic retrofit of RC circular columns using prefabricated composite jacketing. *Journal of structural engineering*, **123**°(10), 1357-1364.

[9] Coffman HL, Marsh ML, Brown CB (1993). Seismic durability of retrofitted reinforced-concrete columns. *Journal of Structural Engineering*, **119**°(5), 1643-1661.

[10] Seible F, Priestley MJN (1993). Retrofit of rectangular flexural columns with composite fiber jackets. *2th Annual Seismic Research Workshop*, Sacramento, California.

[11] Park R, Rodriguez ME., Dekker DR (1993). Assessment and retrofit of a reinforced concrete bridge pier for seismic resistance. *Earthquake spectra*, **9**°(4), 781-801.

[12] Yeh YK, Mo YL., Yang CY (2002). Seismic performance of rectangular hollow bridge columns. *Journal of Structural Engineering*, **128**°(1), 60-68.

[13] Pinto AV, Molina J, Tsionis G (2003). Cyclic tests on large-scale models of existing bridge piers with rectangular hollow cross-section. *Earthquake engineering & structural dynamics*, **32**°(13), 1995-2012.

[14] Calvi G, Pavese A, Rasulo A, Bolognini D (2005). Experimental and numerical studies on the seismic response of RC hollow bridge piers. *Bulletin of Earthquake Engineering*, **3**°(3), 267-297.

[15] RT D.1.2 – part 1 (2015). Inventory e sviluppo database per la caratterizzazione della vulnerabilità delle infrastrutture viarie. *STRIT Project ''PON Ricerca e Competitività 2007-2013"*

[16] Federation Internationale du Beton (2007). Seismic bridge design and retrofit—structural solutions. *FIB Bulletin 39*.